INTELLIGENT AUTOMATION & SOFT COMPUTING, 2017
http://dx.doi.org/10.1080/10798587.2016.1267240

Meteorological Correction Model of IBIS-L System in the Slope Deformation Monitoring

Xiaoqing Zuo[a], Hongchu Yu[a], Chenbo Zi[b], Xiaokun Xu[b], Liqi Wang[b] and Haibo Liu[b]

[a]Faculty of Land and Resource Engineering, Kunming University of Science and Technology, Yunnan Province, China; [b]Huaneng Lancang River Hydropower CO., LTD, Kunming City, Yunan Province, China

ABSTRACT

Micro deformation monitoring system (IBIS-L) using high frequency microwave as signal for transmission, is easily affected by meteorology. How to eliminate the meteorological influence effectively, and extract useful information from the big data becomes a key to monitor the slope deformation with high precision by the IBIS-L system. Evaluation of the optimum meteorological correction mode for Slope Deformation Monitoring to ensure the accuracy of measurement is considered. This objective was realized by model construction technology, which uses calculation formula of Microwave Refraction rate, and the radial distance from the target point to the IBIS-L system to estimate the irreal displacement by meteorological influence. In this paper we examine feasibility and accuracy of the meteorological correction model via experiment analysis. This experiment takes the Nuozhadu hydropower station slope monitoring for example. Firstly, the temperature, humidity, air pressure and other meteorological parameters were measured simultaneously with IBIS-L system monitoring. Secondly, the measured meteorological parameters were taken into calculation formula of Microwave Refraction rate. Thirdly, combined with the radial distance from the target point to the IBIS-L system, the meteorological correction model in using IBIS-L system for slope deformation monitoring was established.

KEYWORDS

IBIS-L system; slope deformation monitoring; big data; meteorological correction model

1. Introduction

Conventional monitoring techniques, such as inclinometers, extensometers, GPS or terrain surveys only provides displacement information of a limited number of points in the landslide zone, but ground-based synthetic aperture radar interferometry technique has proven its ability to monitoring across displacement, widely used in glacier, volcanoes and other landslides monitoring and disaster warning (Fang & Xu, 2012). In addition, ground-based radar interferometry technique is not affected by illumination and climate, unlike space-borne radar under the influence of the carrying platform and satellite parameters without high accuracy (Sabine, Matthias, Carl, et al., 2010). Micro deformation monitoring system (IBIS-L) using stepped frequency microwave as the signal for transmission, susceptible to humidity, temperature, air pressure and other atmospheric factors. How to eliminate atmospheric disturbance, becomes the key for the IBIS-L system to achieve high-precision measurements.

Foreign scholars (Lu & Noferini, 2009) analyzed the effect of the changes of atmospheric water vapor content in time and space on ground-based interferometry, put forward two correction methods by the external auxiliary data and permanent scattered technique, and successfully applied to the landslides monitoring of Citrine Valley in Italy. Iannini & Monti (2011) took the means of statistical analysis, obtained phase change caused by atmospheric effects in ground-based radar interferometry, and gave the corresponding compensation. Domestic scholars Zhang, Lu, & Song (2011) using the corner reflectors as stability control points, analyzed atmospheric disturbance change in monitoring areas and corrected the disturbance errors, but the atmospheric variation along propagation path was simple to be considered as uniform during the observation, only suitable for short distance observation within 100 meters. Xu, Zhou, Wang, & Xing (2013) put forward a global environmental correction method based on the discrete stable point, but only suitable for small areas. Hua, Li, Hu, et al. (2013) studied the influencing factors of correction methods of determination atmospheric parameters and selection the stable points, and analyzed their advantages and disadvantages, experiments show that these two methods can effectively correct the environmental impact in short time and short distance observation.

Each of the previously mentioned ground radar interferometry meteorological influence calibration methods has its own unique advantages, but it also has obvious shortcomings: (1) PS technology can solve the issues of space irrelevant and time irrelevant, but requires large amounts of data, the data processing is complex, and it is only suitable for a small range area with smooth and continuous deformation. (2) The existing atmospheric model correction method, of which the atmospheric variation along a propagation path is simple to be considered as uniform during the observation, is only suitable for short distance observation within 100 meters. (3) External auxiliary data for calibration, depending on the accuracy of external data and interpolation algorithm, and the auxiliary data with the same resolution of the SAR image is difficult to obtain.

CONTACT Hongchu Yu hongshuxifan8140@163.com

Aiming at the existing problems and shortcomings of the existing technology, this paper provides a Meteorological correction model for slope deformation monitoring. This model combines the microwave refractive index change and ground-based radar interferometry principle, uses experimental analysis and nonlinear fitting method, and can effectively correct meteorological influence. The model overcomes the problem that the atmospheric variation along the propagation path is simple to be considered as uniform during the observation, and is suitable for the slope deformation monitoring in the range of a1000 meters. Compared with the previous calibration model within 100 meters, this model is more practical and reliable. To further verify the validity of the model, experiments are carried out in Nuozhadu. Because water vapor distribution of Nuozhadu hydropower station slope is very complex and changeable, atmospheric effects in a few hours will produce centimeter-level additional displacement, which cannot be ignored. Only by effectively eliminating the meteorological influence can we achieve the high precision monitoring requirements of sub-millimeter.

2. IBIS-L System Monitoring Principle

The micro deformation monitoring system (IBIS-L) uses synthetic aperture radar, interferometry, and stepped frequency continuous wave and other advanced technology to obtain high-precision, high-resolution deformation information. Among them, the step frequency continuous wave and synthetic aperture radar technology used to improve range resolution and azimuth resolution of radar images, and interferometric techniques were used to extract deformation information (Richards, 2001).

(1) Synthetic aperture radar technology

Synthetic aperture radar technology uses phase information of synthetic aperture radar to extract large-scale, high-precision, all-weather and three dimensional change information of target. When the antenna of IBIS-L system is scanning along the track, which is equivalent to increase antenna aperture, the angle resolution can be increased to 4.4mrad (Satoshi, Koji, & Koji, 2011).

(2) Interferometry

Each measurement of the target includes both information of the amplitude$|I(n)|$and the phase ϕ_n. Interferometry Technology provides the change amount of displacement through analysis of difference in phase information of the target reflected wave obtained by the radar system at different times. $d = -\lambda \div 4\pi * (\varphi_2 - \varphi_1)$, d is the displacement change, λ as radar wavelength, $\varphi_2 - \varphi_1$ for radar wave phase difference (Li, Fielding, Cross, & Muller, 2006 and Linhsia, Daniele, Giovanni, et al., 2009).

(3) Stepped frequency continuous wave technology

Launching N sets of electromagnetic waves with continuous frequency at the same time, the pulse duration of each set electromagnetic wave is T (Deepika, Iaeng, & Manabendra, 2015).

It provides high range resolution for the radar. The radar is able to provide a maximum frequency bandwidth of 3×10^8, the range resolution of 0.5 m obtained by $\Delta r = C \div 2B$. According to the resolution, in the radar monitoring area, every 0.5 m along the radar sight direction is divided into a monitoring unit (He, Luo, Huang, et al., 2007 and Zuo, Yan, Wei, Li, & Y, 2014).

3. Meteorological Correction Model of Slope Deformation Monitoring

In radar interferometry, the meteorology influence on the electromagnetic wave propagation is mainly to produce refraction, which leads to the radar phase delay, and the irreal formation displacement. So the change of the atmospheric refractive index n has a significant effect on the interference phase. The radar wave is a kind of microwave, propagating medium is troposphere, and the refractive index n is related to the temperature, the pressure and the humidity. The further calculation process of atmospheric refraction index is as follows:

The formula of saturation vapor pressure on the horizontal plane was recommended by the World Meteorological Organization (1966).

$$\begin{aligned}\lg e &= 10.75947\left(1-\tfrac{T_1}{T}\right) - 5.02800\lg\tfrac{T_1}{T} \\ &+ 1.50475\times10^{-4}\left[1-10^{-8.2969\left(\frac{T}{T_1}-1\right)}\right] \\ &+ 4.2873\times10^{-4}\left[10^{4.69455\left(1-\frac{T}{T_1}\right)}-1\right] + 0.78614\end{aligned} \tag{1}$$

where lg represents the logarithm, lg e represents the logarithm of e, and e is the saturation vapor pressure on the horizontal plane; T_1 is 273.16 K; $T = 273.15 + t$, t is the measured temperature (°C), and the scope of t is −49.9– 49.9 °C.

There is a difference between moist air saturation water vapor pressure, also known as effective saturation vapor pressure, and saturation vapor pressure on the horizontal plane. According to the World Meteorological Organization (WMO), moist air saturation vapor pressure was calculated using the following formula.

$$\begin{aligned}e'(t) &= f(P)\cdot e(t) \\ f(P) &= 1.0016 + 3.15\cdot10^{-6}P - 0.074P^{-1}\end{aligned} \tag{2}$$

Where $e'(t)$represents moist air saturation water vapor pressure, in unit of hpa; P is the measured air pressure, in unit of hpa; $e(t)$ is saturation vapor pressure on the horizontal plane calculated by the formula(1), the unit is hpa;

Microwave refractive index was calculated using Essen-Froome empirical formula recommended by the international Union of Geodesy and Geophysics (IUGG, 1963).

$$\left(n_{t,p,e}-1\right)\cdot10^6 = \frac{103.49}{T}P_1 + \frac{177.4}{T}P_2 + \frac{86.26}{T}\left(1+\frac{5,748}{T}\right)e' \tag{3}$$

where $n_{t,p,e} - 1$ indicates that the difference between the refractive index and one, dimensionless, and $e'$is the water vapor pressure, which is calculated according to the moist air saturation vapor pressure computed by preceding formula (2) and air relative humidity. P_2 for the partial pressure of CO_2, according to the CO_2 content in the air, calculate the corresponding carbon dioxide partial pressure P_2, such as the industry in Yunnan Province is not developed, the content of CO_2 in air is about 0.03%, and the corresponding carbon dioxide partial pressure is $P \div 100 * 0.03$; P_1 is partial pressure of dry air, without CO_2, $P_1 = P - P_2 - e'$, P is the measured pressure.

According to electromagnetic theory, the frequency of radar wave IBIS-L emitted is f, and the echo phase of target point with distance of R can be expressed as $\varphi(t) = (4\pi f \div c)\int n(R, t)d_R$, where c is the speed of light in vacuum, n for the refraction rate. The phase delay of the stable point in the scene is related to refractive index n and the radial distance R. According to

Table 1. The Refractive Index Change on September 10th, on September 18th, and on September 24th.

September 10th					September 18th					September 24th				
time	*T*	*P*	*H*	$R(*10^{-3})$	time	*T*	*P*	*H*	$R(*10^{-3})$	time	*T*	*P*	*H*	$R(*10^{-3})$
16.110,6	31.5	922.9	0.371,7	0. 000	16.152,0	30.4	925.1	0.667,8	0.000	16.110,6	34	924.7	0.399,6	0. 000
16.208,4	31.7	922.7	0.365,1	−0. 449	16.249,8	30.4	925.1	0.667,8	0.000	16.208,4	34.9	924.8	0.369,2	−2. 114
16.306,1	31.7	922.5	0.365,1	−0. 497	16.347,6	30.5	925	0.661,8	−0. 307	16.306,1	33.8	924.7	0.406,7	0. 477
16.403,9	31.6	922.4	0.368,4	−0. 321	16.445,3	30.4	925	0.667,8	−0. 024	16.403,9	33.1	924.8	0.432,6	2. 179
16.501,7	31.5	922.4	0.371,7	−0. 121	16.543,1	30.4	924.9	0.667,8	−0. 049	16.501,7	32	924.8	0.477,1	4. 836
16.599,5	31.7	922.3	0.365,1	−0. 545	16.640,9	30.5	924.9	0.661,8	−0. 331	16.599,5	31.2	924.8	0.512,4	6. 785
16.697,3	32	922.3	0.355,5	−1. 144	16.738,7	30.8	925	0.644,2	−1. 154	16.697,3	30.8	924.9	0.531,1	7. 789
16.795,0	32.1	922.1	0.352,3	−1. 392	16.836,5	30.9	925	0.638,4	−1. 436	16.795,0	31.2	924.9	0.512,4	6.810
16.892,8	32.3	922	0.346,1	−1. 814	16.934,2	30.8	925	0.644,2	−1. 154	16.892,8	31.3	925	0.507,8	6. 589
16.990,6	32.7	921.9	0.334,0	−2. 632	17.032,0	30.5	925.1	0.661,8	−0. 283	16.990,6	31.6	925	0.494,4	5. 858
17.088,4	33.2	921.9	0.319,6	−3. 620	17.129,8	30.4	925.2	0.667,8	0. 024	17.088,4	31.8	924.9	0.485,6	5. 347
17.186,1	33.5	921.8	0.311,2	−4. 235	17.227,6	30.1	925.2	0.686,1	0. 874	17.186,1	31.3	924.9	0.507,8	6. 565
17.283,9	33.7	921.8	0.305,7	−4. 628	17.325,3	29.9	925.3	0.698,6	1. 466	17.283,9	31.2	924.9	0.512,4	6. 810

the measured meteorological parameters, such as temperature, humidity and air pressure, calculate the change in atmospheric refractive index, combined with the radial distance from the target point to IBIS-L system and the additional displacement by atmospheric effects, establish meteorological correction model. Because the distance between IBIS-L system and Nuozhadu hydropower station slope ranges from 500 to1000 *m*, atmospheric changes on the propagation path during the observation period cannot be simply regarded as uniform. The experiments demonstrated Nuozhadu hydropower station in proximity of atmospheric conditions every 300 meters. In the range of one kilometer, the increase of the radial distance accelerates the rate of the additional displacement growth caused by the atmospheric influence, therefore set 300, 600 and 900 m as the critical value, the deformation in the direction of the radar line of sight caused by atmospheric effects is

$$d = \begin{Bmatrix} \Delta nR(0 < R \leq 300) \\ \Delta n * 300 + 2 * \Delta n * (R - 300)(300 < R \leq 600) \\ \Delta n * 300 + 2 * \Delta n * 300 + 3 * \Delta n * (R - 300)(600 < R \leq 900) \\ \Delta n * 300 + 2 * \Delta n * 300 + 3 * \Delta n * 300 + 4 * \Delta n * (R - 300)(900 < R) \end{Bmatrix} \quad (4)$$

Where d expresses the additional displacement caused by meteorological effect, R for radial distance value between radar equipment and monitoring points, and Δn is the change value of refractive index.

4. Experiment Schemes and Data Processing

4.1. Data Acquisition

The IBIS-L system and meteorological monitoring equipment was arranged in the observation station on the other side of the slope. Taking into account stable atmospheric conditions from three pm until the sun goes down, in order to reduce the error of meteorological monitoring, the temperature, pressure and humidity, and other meteorological parameters were monitored during four o'clock to six o'clock in the afternoon on September 10th, September 18th and September 24th, while obtaining radar data.

4.2. Data Processing

4.2.1. IBIS-L System Radar Monitoring Data Processing

(1) Data calibration and focusing processing

Radar data is one-dimensional signal data, through calibration and focus processing to get two-dimensional fan images, which had range resolution of 0.5 m and the azimuth resolution of 4.4 mrad (Liu, 2004).

(2) Interferometric processing

By setting a threshold value (intensity values or coherence generally above 0.5) to remove the points of bad quality, ensure the reliability of the interference images. Data interferometric processing, select a primary image first, then separately interfere with the rest of the images. After interference, set the appropriate filtering window for the filtering processing of the interferogram, to remove the influence of noise, which can ensure the continuity of the phase, accelerate the unwrapping speed and improve accuracy. Phase unwrapping can be carried out after filtering, to obtain the real phase (Hassene, Sondes, & Ezzeddine, 2014).

(3) Differential treatment

With differential processing between every two interferograms, obtain the phase change value in the distance direction at various times and convert into displacement values to get

Table 2. The Information of Corner Reflectors.

Pixel	P1	P2	P3	P4	P5	P6	P7	P8	P9	P10	P11	P12
X[m]	299	248.7	214.9	274.7	267.1	234.7	−205.9	−229.9	−261.5	−287.3	−248.3	−245.2
Y[m]	955.5	971.9	923.5	851.5	894.7	884.6	982.4	1,008.3	508.9	671.3	609.5	572.9
Thermal SNR[dB]	36.1	38.4	36.4	38.1	38	37.3	33.3	34.5	34	31	27.9	27.4
Estimated SNR[dB]	25.3	23.6	25.4	28.5	24.1	26.2	24.4	20.8	21.1	21.1	20.6	20.7
Coherence	0.83	0.83	0.86	0.87	0.85	0.87	0.86	0.86	0.94	0.89	0.9	0.91

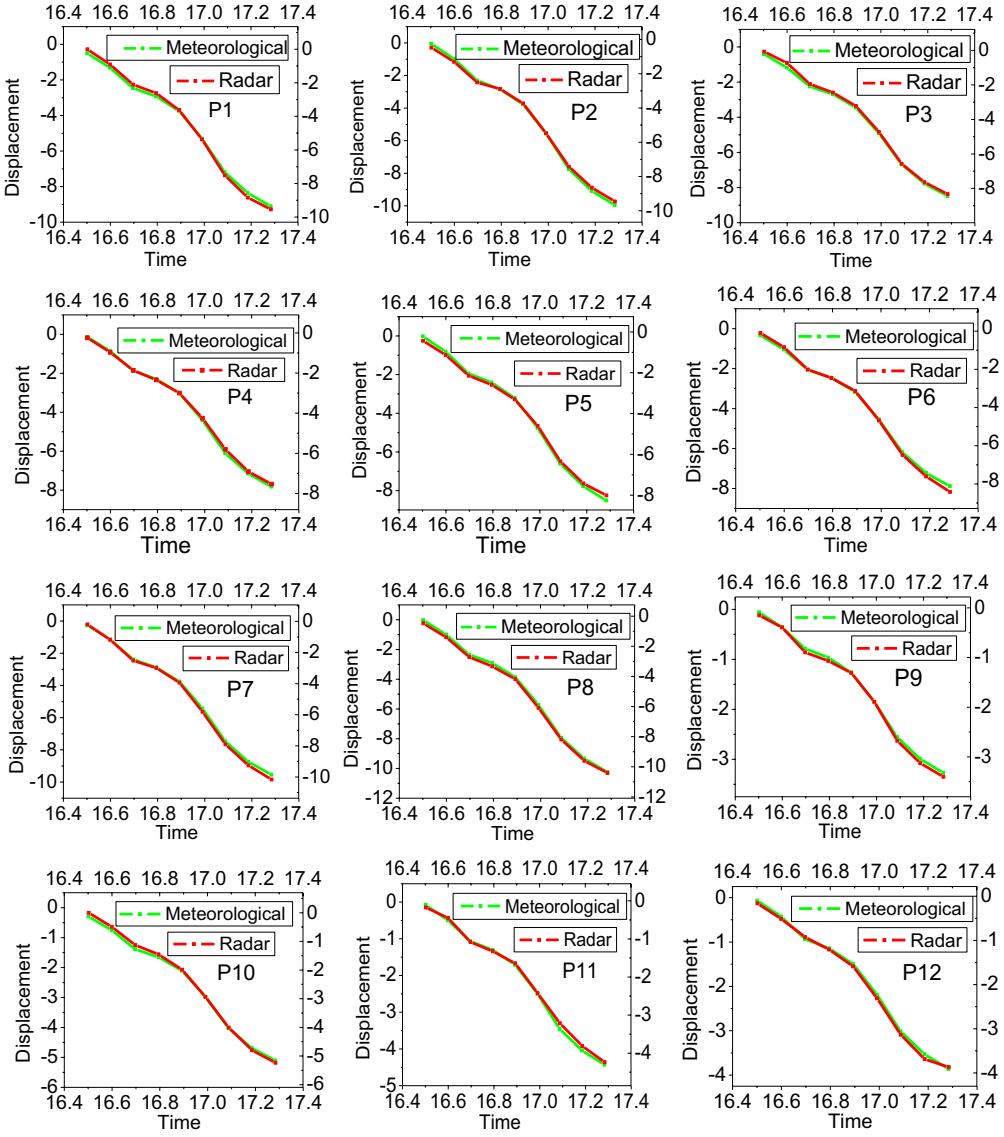

Figure 1. Line Charts of the Additional Displacement by Meteorological Impact and the Delay Displacement Calculated by Meteorological Model on September 10th.

the deformation (Fukuda & Hirosawa, 1999 and Zhang, Wang, & Xu, 2012).

4.2.2. Refractive Index Calculation

Because the distance between the target point and IBIS-L system is less than 1000 m belongs to the short-range observation, so the refractive index within the observing scene can be regarded as the same in a moment, and the spatial variation is ignored. According to the measured temperature (T), barometric pressure (P) and relative humidity (H), calculated the refractive index change value (R), as shown in Table 1. It is obvious that the bigger temperature, relative humidity fluctuates from 16:00 to 17:30 on September 24th, the bigger refractive index change.

4.2.3. Irreal Displacement by Meteorological Influence Correction

Corner reflectors with strong scattering, high correlation, high thermal signal noise ratio (Thermal SNR), and high estimated signal noise ratio (Estimated SNR) can be used as stable points, whose displacement variation was only affected by the atmospheric turbulence. Corner reflectors appeared red on the radar signal noise ratio image, according to contrast the images before and after resettlement, identified all the corner reflectors on the radar image.

The radar coordinate system is a two-dimensional coordinate system, the origin of the coordinate system in the geometric center of the track, the X axis is parallel to the geometrical track, and the Y axis is the direction of the radar line of sight (He & He, 2009 and Sureerat, Konglo, & Nopparat, 2016). Thermal signal to noise ratio represents the reflection quality of electromagnetic waves, the estimated signal to noise ratio on behalf stability of electromagnetic wave, thermal signal to noise ratio above 25 dB is the premise to determine the stability point, but only the point with thermal signal to noise ratio above 25 dB, the estimated signal to noise ratio above 20 dB and the correlation above 0.8, can be determined as the stable point (Crouse, Nowak, & Baraniuk, 1998 and Zebker, Werner, et al., 1994). In the experiment, we placed 12 corner reflectors, whose geometrical position, Thermal SNR, Estimated SNR and correlation information as shown in Table 2.

According to the additional displacement by meteorological impact and the delay displacement calculated by meteorological model of P1 to P12 on the September 10th, September 18th and September 24th, 4 pm to 6 pm, draw line charts, as shown in Figure 1, Figure 2 and Figure 3. The two lines are almost

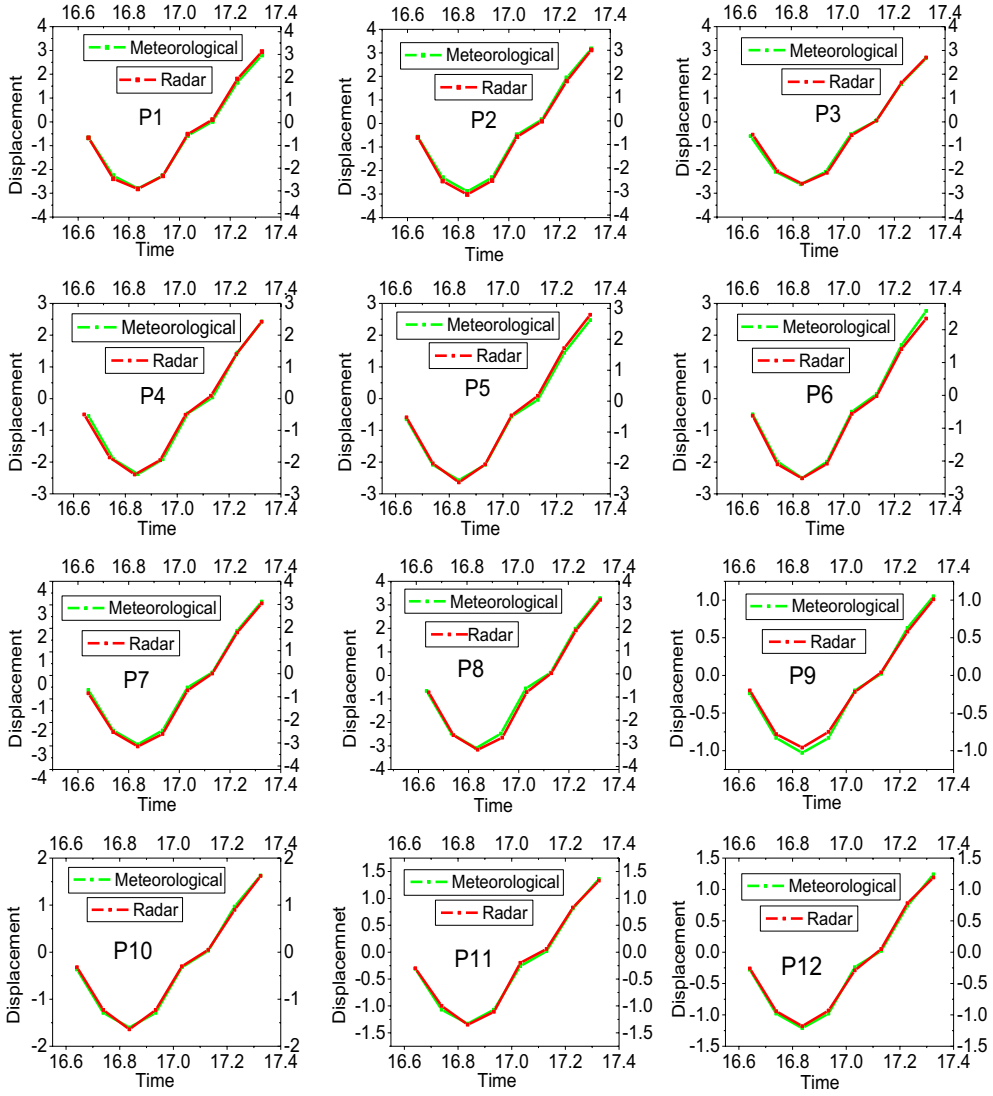

Figure 2. Line Charts of the Additional Displacement by Meteorological Impact and the Delay Displacement Calculated by Meteorological Model on September 18th.

consistent, the difference is small, and the results are good. The two lines cannot be completely consistent, mainly because the meteorological data was measured at the observation station, where meteorological conditions were slightly different from each monitoring point's. The closer the observation point is away from IBIS-L system, the smaller the additional displacement caused by meteorological influence will be, such as p9 to p12. The further the observation point is away from IBIS-L system, the bigger the additional displacement caused by meteorological influence will be, such as p1 to p8. In general, with the increase of the distance between the monitoring points and the radar equipment, the additional displacement caused by meteorological influence has a tendency to accelerate the increase, with nonlinearly related. As P9 508.9 meters from the radar equipment, P8 10,008.3 meters from the radar equipment, but the displacement caused by meteorological influence of P8 is about three times of P9.

According to the additional displacement by meteorological impact and the delay displacement calculated by meteorological model of P1 to P12, calculated the differences between the two displacements, the average, the variance, and the standard deviation of differences, as shown in Table 3. It is not hard to

Table 3. The Table of Statistical Analysis.

	September 10th			September 18th			September 24th		
	Average	Variance	Standard deviation	Average	Variance	Standard deviation	Average	Variance	Standard deviation
P1	0.002,5	0.002,269	0.047,631	0.018,182	0.001,451	0.038,095	−0.002,5	0.001,785	0.042,254
P2	−0.009,17	0.002,574	0.050,738	0.004,545	0.001,916	0.043,769	−0.005	0.001,325	0.036,401
P3	0.01	0.002,967	0.054,467	0.007,273	0.001,638	0.040,472	−0.01	0.001,25	0.035,355
P4	0.002,5	0.001,569	0.039,607	−0.006,36	0.001,478	0.038,441	−0.004,17	0.002,091	0.045,727
P5	−0.01	0.001,367	0.036,968	−0.005,45	0.001,698	0.041,201	0.005	0.001,392	0.037,305
P6	−0.004,17	0.001,258	0.035,463	−0.000,91	0.001,59	0.039,876	−0.010,83	0.001,741	0.041,725
P7	0.022,5	0.000,919	0.030,311	−0.015,45	0.001,588	0.039,855	−0.005	0.001,625	0.040,311
P8	0.01	0.000,95	0.030,822	−0.011,82	0.002,179	0.046,675	−0.005	0.002,008	0.044,814
P9	−0.004,17	0.001,191	0.034,51	0.003,636	0.002,223	0.047,15	0.001,667	0.001,181	0.034,359
P10	−0.008,33	0.001,181	0.034,359	0.000,909	0.001,863	0.043,16	0.006,667	0.001,972	0.044,41
P11	−0.009,17	0.001,708	0.041,324	0.005,455	0.001,461	0.038,225	0	0.001,15	0.033,912
P12	0.005	0.002,592	0.050,908	0.006,364	0.001,223	0.034,973	−0.002,5	0.002,002	0.044,745

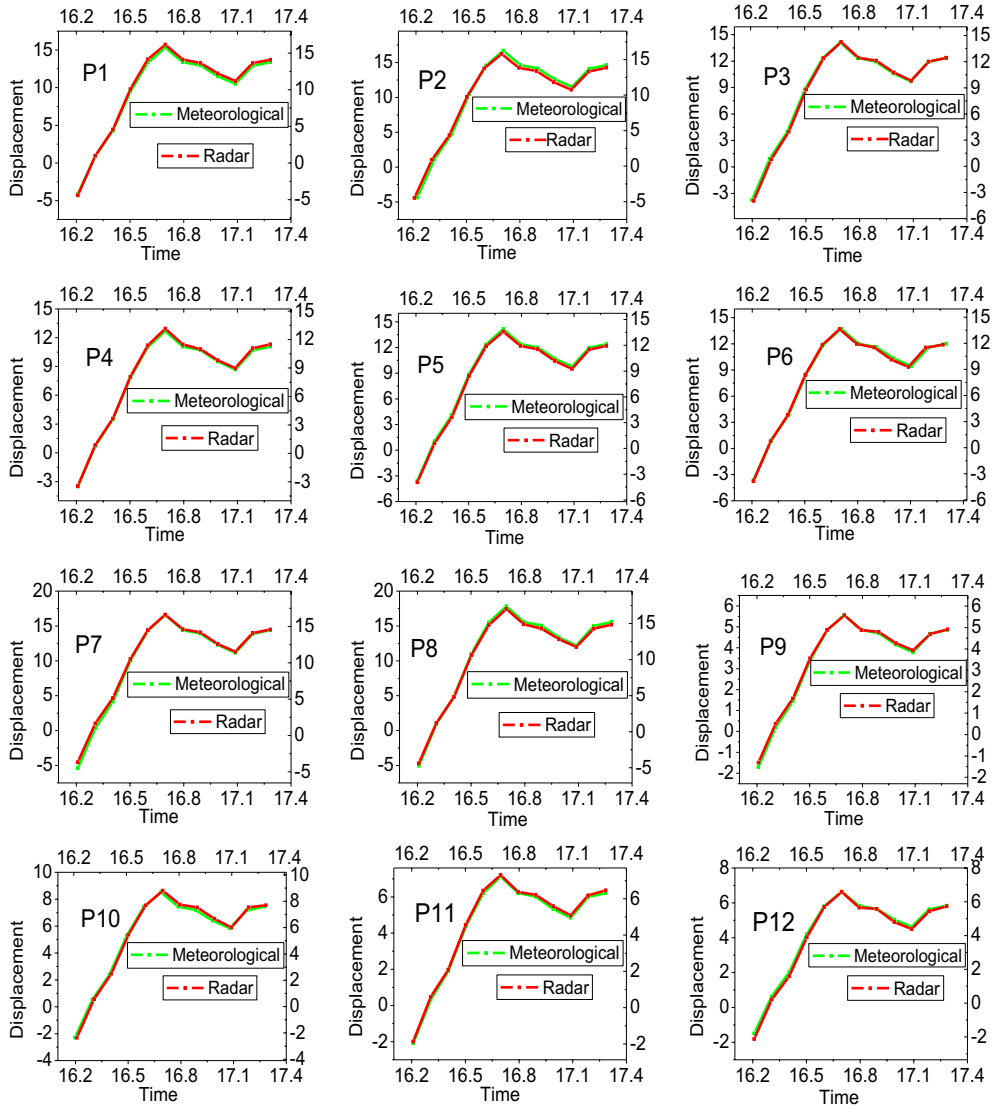

Figure 3. Line Charts of the Additional Displacement by Meteorological Impact and the Delay Displacement Calculated by Meteorological Model on September 24th.

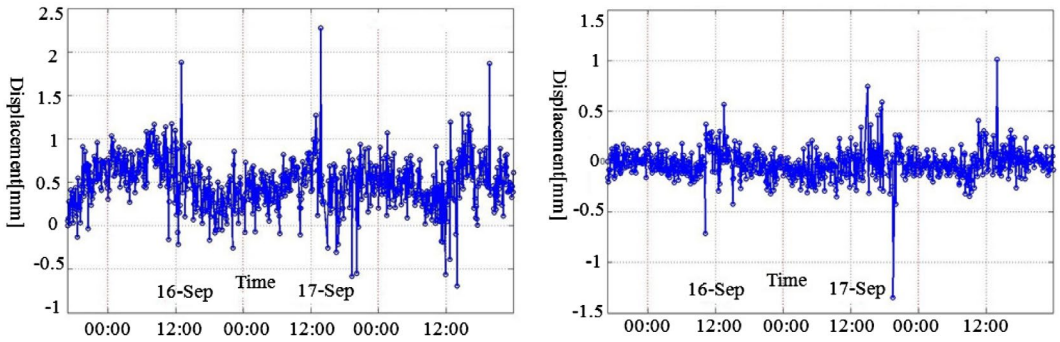

Figure 4. Comparative Analysis Diagram of Meteorological Model Correction and GCP Correction.

see that the average value on September 10th, September 18th and September 24th, within 0.1 mm, the variance and standard deviation are relatively small, indicating that the meteorological correction model has high accuracy and good effect. In ground-based radar interferometry, under relatively stable monitoring environmental conditions, using more sophisticated atmospheric parameters measuring equipment, meteorological influence correction method by measuring atmospheric parameters is very effective, which can achieve high-precision surface monitoring.

4.2.4. Comparative Analysis

Collecting the radar data of a suitable target on September 16, September 17 and September 18, then using permanent scattered technique and the meteorological correction model constructed in this paper to correct the displacement caused by the impact of meteorological, the corrected results are shown in Figure 4, the left part for the displacement change trend after GCP corrected, the right part for the displacement change trend after meteorological correction model amended. In comparison with the change trend of displacement by GCP

corrected, the change trend of displacement by the meteorological model corrected with smaller fluctuation, it is obviously that, meteorological Correction model has high precision, can effectively correct the irreal displacement caused by meteorological effection.

5. Conclusions and Discussion

This paper focuses on correction model in using IBIS-L system for slope deformation monitoring. First of all, corner reflectors placed on the slope as stable points, the IBIS-L system monitoring and temperature, humidity and air pressure and other meteorological parameters measured simultaneously, calculated refractive index change, combined with the displacement from meteorological impact by IBIS-L monitoring, to establish meteorological correction model. The results show that the model can effectively correct meteorological influence, attain sub-millimeter accuracy in the radar sight direction, and achieve high-precision surface monitoring. However, atmospheric parameters comparatively stable in the monitoring time from 16:00 to 17:30, how to get the all day's meteorological correction model need further study.

Acknowledgments

The authors would like to thank Huaneng Lancang River Hydropower CO., LTD for supporting this research effectively. We wish to acknowledge the editor, associate editor, reviewers and anonymous referees for their essential contribution which have been very helpful in enhancing the quality of this paper.

Disclosure statement

No potential conflict of interest was reported by the authors.

Notes on contributors

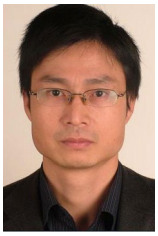

Xiaoqing Zuo received a PhD degree in surveying and mapping engineering in 2004, and is now a professor at Kunming University of Science and Technology. His research interests include remote sensing image processing, spatio-temporal data mining and ground-based interferometric synthetic aperture radar.

Hongchu Yu obtained MS degree in Surveying and Mapping Engineering from the Faculty of Land and Resource Engineering at Kunming University of Science and Technology, China. Her field of research includes remote sensing image processing, spatio-temporal data mining and data acquisition and processing in ground-based radar monitoring, in which areas she has published 4 journal papers and one conference paper.

Chenbo Zi obtained MS from the Faculty of Land and Resource Engineering at Kunming University of Science and Technology in 2001, and at present, is a Senior Engineer in Reservoir operation and security administration field. He served as Deputy Director at Reservoir section in Nuozhadu Hydropower station, now is the Director in Nuozhadu Hydropower station.

Xiaokun Xu obtained BS in Water Conservancy and Hydropower Construction Engineering from The North China Institute of Water Conservancy and Hydroelectric Power (NCWU) in 2001 and, at present, is a Senior Engineer in Reservoir operation and security administration field. He started work in July 2001, and served as technician, technical director at Gezhouba Group test center, and as a project manager In Gezhouba Dam Group Testing Co. Ltd. He served as header of hydraulic group at Production Preparation Department and served as the assistant of Director in Nuozhadu Hydropower preparatory office. Now He is the assistant of Director at Reservoir section in Nuozhadu Hydropower station.

Liqi Wang obtained his BS in Water Conservancy and Hydropower Engineering from China Three Gorges University in 2009. At present, is a Mid-level Engineer in Huaneng Lancang River Hydropower CO. LTD, mainly engaged in the study on safety monitoring of hydraulic structures and operation of hydraulic structures.

Haibo Liu obtained his MS in Water Conservancy and Hydropower Engineering from Kunming University of Science and Technology. At present, is a Mid-level Engineer in Huaneng Lancang River Hydro power CO. LTD, mainly engaged in the study on safety monitoring of hydraulic structures and application of hydraulic structures.

References

Crouse, M.S., Nowak, R.D., & Baraniuk, R.G. (1998). Wave-based statistical signal processing using hidden Markov model [J]. *IEEE Transactions on Signal Processing, 46*, 886–902.

Deepika, H., Iaeng, V.K.N., & Manabendra, B. (2015). SAR image despeckling based on lapped transform domain dual local wiener filtering framework [j]. *IAENG International Journal of Computer Science, 42*, 113–126

Fang, W.H., & Xu, L.Y. (2012). Multi-scale model of Dam safety condition monitoring based on dynamic bayesian networks [J]. *Intelligent Automation & Soft Computing, 18*, 909–921.

Fukuda, S., & Hirosawa, H. (1999). A wavelet-based texture feature set applied to classification of multifrequency polarimetric SAR images [J]. *IEEE Transactions on Geoscience and Remote Sensing, 37*, 2282–2286.

Hassene, S., Sondes, T., & Ezzeddine, B.B. (2014). Smart real time adaptive gaussian filter supervised neural network for efficient gray scale and RGB image de-noising [J]. *Intelligent Automation & Soft Computing, 20*, 347–364.

He, M., & He, X.F. (2009). Urban change detection using coherence and intensity characteristics of multi-temporal SAR imagery[C]. Xi'an:2nd Asian-Pacific conference on Synthtic Aperture Radar.

He, X.F., Luo, H.B., Huang, Q.H., & He, M. (2007). Integration of InSAR and GPS for hydraulic engineering [J]. *Science in China Series E: Technological Sciences, 50* (Supp.I):111–124.

Hua, Y.F., Li, L.Y., Hu, W.S., Jin, X.H., & Sun, T.K. (2013). Environment correction methods of static micro-deformation surveyed by ground-based radar[J]. *Journal of Southeast University (Natural Science Edition), 43*, 428–432.

Iannini, L., & Monti Guarnieri, A. (2011). Atmospheric phase screen in ground-based radar: Statistics and compensation [J]. *IEEE Geoscience and Remote Sensing Letters, 8*, 537–541.

International Union of Geodesy and Geophysics. (1963). *Comptes rendus de la XIIIe Assemblée Générale de l.* U.G.G.I. Berkeley, California, United States. 1963, S. 15.

Li, Z.H., Fielding, E.J., Cross, P., & Muller, J.P. (2006). Interferometrics synthetic aperture radar atmospheric correction: Medium Resolution Imaging Spectrometer and Advanced Synthetic Aperture Radar integration [J]. *Geophysical Research Letters, 33*, 816–820.

Linhsia, N., Daniele, M., Giovanni, M., & Atzeni, C. (2009). Monitoring of belvedere glacier using a wide angle GB-SAR interferometer [J]. *Journal of Applied Geophysics, 68*, 289–293.

Liu, G.X. (2004). *Mapping of earth deformation with satellite SAR interferometry: A study of its accuracy and reliability performance [D]*. Hong Kong: Hong Kong Polytechnic University.

Lu, Z.G., Noferini, L., Mecatti, D., Macaluso, G., Pieraccini, M., Atzeni, C., … & Nagler, T. (2009). Using a ground based SAR interferometer and a terrestrial laser scanner to monitor a snow-covered slope: Results from an experimental data collection in tyrol (Austria) [J]. *IEEE Transactions on Geoscience and Remote Sensing, 47*, 382–393.

Richards, J.A. (2001).Target model generation from multiple synthetic aperture radar images, *Ph.D. dissertation, Dept. Electron. Eng. Comput. Sci.,MIT*, Cambridge, MA, 2001.

Sabine, R.., Matthias, B., Carl, G., & Steineck, D. (2010). Digital elevation model with the ground-based SAR IBIS-L as basis for volcanic deformation monitoring [J]. *Journal of Geodynamics, 49*, 241–246 .

Satoshi, H., Koji, W., & Koji, O. (2011). One mapping and blending method to improve SAR image visibility [J]. *IAENG International Journal of Computer Science, 38*, 117–123.

Sureerat, A., Konglo, K., & Nopparat, P. (2016). Numerical computations of three-dimensional air-quality model with variations on atmospheric stability classes and wind velocities using fractional step method [J]. *IAENG International Journal of Applied Mathematics, 46*(1), 155–164.

World Meteorological Organization (1966). General meteorological standards and recommended practices. Appendix A. WMO Technical Regulations, WMO-No. 49.

Xu, Y.M., Zhou, X., Wang, P., Xing, C. (2013). Environmental correction methods for ground-based radar interferometry measuring[J] . *Journal of Geodesy and Geodynamics, 33*:41–43, 51

Zebker, H.A., Werner, C.L., Rosen, P. A., & Hensley, S. (1994). Accuracy of topographic maps derived from ERS-1 interferometric radar. *IEEE Transactions on Geoscience and Remote Sensing, 32*, 823–836.

Zhang, X., Lu, B.Y., Song, Q. (2011). atmospheric disturbance correction in ground-based SAR differential interferometry [J]. *Radar Science and Technology*, 9, 502-506,512

Zhang, Z., Wang, X., & Xu, L.Z . (2012). Target detection in sar images based on sub-aperture coherence and phase congruency. *Intelligent Automation & Soft Computing*. *18*, 831–843.

Zuo, T.F., Yan, W.B., Wei, X.Y., Li, Z.L., & Y, G.C. (2014). An effective collaborative filtering via enhanced similarity and probability interval prediction [J]. *Intelligent Automation & Soft Computing*, *20*, 555–566